Calcium hydrazinidoborane: Synthesis, characterization, and promises for hydrogen storage

Salem Ould-Amara, Vibhav Yadav, Eddy Petit, Guillaume Maurin, Pascal Yot, Umit Demirci

HAL Id: hal-02494011

https://hal.umontpellier.fr/hal-02494011

Submitted on 21 Jul 2022

Calcium hydrazinidoborane: synthesis, characterization, and promises for hydrogen storage

Salem OULD-AMARA,[1] Vibhav YADAV,[2] Eddy PETIT,[1] Guillaume MAURIN,[2] Pascal G. YOT,[2,*] Umit B. DEMIRCI [1,*]

[1]   Institut Européen des Membranes, IEM – UMR 5635, Univ Montpellier, CNRS, ENSCM, Montpellier, France

[2]   Institut Charles Gerhardt Montpellier, ICGM – UMR 5253, Univ Montpellier, CNRS, ENSCM, Montpellier, France

*   umit.demirci@umontpellier; pascal.yot@umontpellier.fr

Abstract

Viewing calcium hydrazinidoborane $Ca(N_2H_3BH_3)_2$ (9.3 wt% H) as a potential hydrogen storage material, we long sought to synthesize it by solid-solid reaction of calcium hydride CaH_2 and hydrazine borane $N_2H_4BH_3$. However, it was elusive because of unsuitable experimental conditions. In situ synchrotron thermodiffraction helped us to identify the key role played by the temperature in the formation of the new phase. From 45°C, new diffraction peaks appear, and the DSC analysis shows an exothermic signal. Thermal activation is thus required to make solid-state CaH_2 react with melted (liquid-state) $N_2H_4BH_3$. The XRD pattern can be indexed using a mixture of two phases: (*i*) unreacted CaH_2 as a minor phase (29 wt%) and (*ii*) the hitherto elusive $Ca(N_2H_3BH_3)_2$ (71 wt%). The as-formed $Ca(N_2H_3BH_3)_2$ crystallizes in a monoclinic *Ic* (No. 9) unit cell where the intermolecular interactions form chains (layers) along the *a* axis, resulting in intra-chain and inter-chain Ca···Ca distances as short as 4.39 and 7.04 Å respectively. Beyond 90°C, $Ca(N_2H_3BH_3)_2$ decomposes, as evidenced by the diffraction peaks fading, an exothermic signal revealed by DSC, a weight loss (5.3 wt% at 200°C) observed by TGA, and a gas release (H_2, and some N_2, NH_3, N_2H_4) monitored by MS. The as-formed thermolytic residue is amorphous and of complex polymeric composition. These results and the next challenges, are discussed herein.

Keywords

Calcium hydrazinidoborane; Dehydrogenation; Hydrazine borane; Hydrogen storage.

1

1. Introduction

In the field of chemical hydrogen storage, B-N-H materials emerged as promising candidates. They draw their strength from high gravimetric hydrogen densities as well as the concomitant existence of $B-H^{\delta-}$ and $N-H^{\delta+}$ bonds resulting in heteropolar dihydrogen $B-H^{\delta-}\cdots H^{\delta+}-N$ interactions which drive their solid state at ambient conditions and their ability to release H_2 at relatively mild conditions. A typical representative of B-N-H materials is ammonia borane NH_3BH_3 (AB), composed of 19.5 wt% of hydrogen [1-4]. In pristine state, AB decomposes more than it dehydrogenates, and is not suitable for the targeted application [5-8]. A number of derivatives has been further developed. The strategy is to substitute one $H^{\delta+}$ of the NH_3 group of AB by a cation to form alkali and alkaline-earth amidoboranes $M(NH_2BH_3)_n$, with M^{n+} being e.g. Li^+, Na^+, Mg^{2+}, or Ca^{2+} [9,10]. The idea is to destabilize the anionic entity $[NH_2BH_3]^-$ so that the ionic solid $M(NH_2BH_3)_n$ releases pure H_2 at temperatures lower than those required for AB decomposition. A typical example is sodium amidoborane $NaNH_2BH_3$ (9.5 wt% H) that starts to dehydrogenate at about 50°C and is able to release 7.5 wt% H (2 equiv H_2) up to 200°C [11].

Another representative of B-N-H materials is hydrazine borane $N_2H_4BH_3$ (HB), composed of 15.4 wt% of hydrogen [12]. HB is a derivative of AB, the NH_3 of which being substituted by N_2H_4. Yet, HB, in pristine state, is not suitable for hydrogen storage because, under heating, it releases N_2H_4 together with H_2, and it generates a shock-sensitive solid when heated above 300°C [13]. Alkali hydrazinidoboranes $NH_2NH(M)BH_3$ (or $MN_2H_3BH_3$; denoted MHB) were synthesized by reaction of HB with an alkali hydride MH in such a way that one $H^{\delta+}$ of the middle NH_2 was substituted by M^+ [14]:

$$MH\ (s) + NH_2NH_2BH_3\ (s) \rightarrow NH_2NH(M)BH_3\ (s) + H_2\ (g) \tag{1}$$
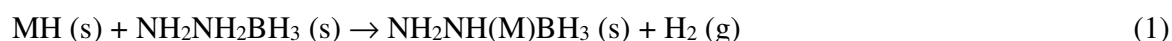
MHB is an ionic solid [15]. Compared to HB, the $B-H$ and $N-H$ bonds of MHB are weaker, which results in more attractive dehydrogenation properties [16]. To date, four MHBs have been successfully synthesized.

The first example of MHB is the polymorphic $LiN_2H_3BH_3$ (denoted LiHB), prepared by ball-milling equimolar amounts of HB and LiH [17,18]. The low-temperature β phase (orthorhombic, s.g. *Pbca*) transforms into the metastable high-temperature α phase (monoclinic, s.g. $P2_1/c$) at around 90°C [19]. LiHB is able to release about 2.5 equiv H_2 when heated up to 150°C (i.e. 9.9

wt% H released, out of a gravimetric hydrogen density of 11.7 wt% H). The second example is $NaN_2H_3BH_3$ (NaHB; monoclinic, s.g. $P2_1/n$) [20]. NaHB is prepared at a temperature below $-30°C$ because the reaction of HB with NaH is exothermic (-27.8 kJ mol^{-1}) [21]. NaHB is less stable than LiHB: it releases H_2 from about 60 °C, with about 2.6 equiv H_2 generated up to 150°C (i.e. 7.6 wt% H released, out of a gravimetric hydrogen density of 8.9 wt% H). The third example is $KN_2H_3BH_3$ (KHB; monoclinic, s.g. $P2_1$). It is synthesized in high pressure vessel and tetrahydrofuran [22], since the solid state reaction between HB and KH is violent (-70.2 kJ mol^{-1}) [21]. KHB, less stable than the previous hydrazinidoboranes, starts to dehydrogenate below 50°C and, cumulatively, about 2.5 equiv H_2 are released up to 193°C (i.e. 6 wt% H released, out of a gravimetric hydrogen density of 7.2 wt% H). The fourth and last example is $RbN_2H_3BH_3$ (monoclinic, s.g. $P2_1$) [23]. Its dehydrogenation properties are favorably compared to those of LiHB. However, with a gravimetric hydrogen density of 4.65 wt% H and a very low terrestrial abundance of the element Rb, the potential of RbHB as hydrogen carrier appears to be rather limited.

To date, alkaline-earth hydrazinidoboranes $M(N_2H_3BH_3)_2$ (denoted $M(HB)_2$, with M^{2+} = e.g. Mg^{2+}, Ca^{2+}) have not been properly considered and really investigated. Advantageously, they carry more hydrogen than NaHB (8.9 wt% H) and KH (7.2 wt% H) do; for instance, the theoretical gravimetric hydrogen densities of $Mg(HB)_2$ and $Ca(HB)_2$ are calculated to be 10.6 and 9.3 wt% H respectively. Another attractive feature is that calcium is, on earth, the most abundant element of the periodic table s block. One has to mention one study that reports the possible synthesis of $Ca(HB)_2$ through an X-ray diffraction pattern that has not been refined and solved [17]. In a previous work [21], we tried to get such a $Ca(HB)_2$ derivative by ball milling one equivalent of CaH_2 and 2 equivalents of HB at different milling conditions. However, all of our attempts failed. Soft ball milling conditions (e.g. 200 rpm for 10 min) resulted in binary mixtures of unreacted starting materials whereas harsher conditions (e.g. 450 rpm for 30 min) led to decomposition of HB into an amorphous polymeric solid. Consequently, we integrated another variable, the temperature. We focused our efforts in following the temperature-dependent evolution of the binary mixture CaH_2-2HB by synchrotron X-ray thermodiffraction and differential scanning calorimetry. Our approach met with the successful synthesis of the first representative of alkaline-earth hydrazinidoboranes, i.e. calcium hydrazinidoborane $Ca(N_2H_3BH_3)_2$ (denoted $Ca(HB)_2$), as described below. $Ca(HB)_2$ was fully characterized by X-

ray diffraction, magic-angle spinning nuclear magnetic resonance spectroscopy, and Fourier transform infrared spectroscopy, and its dehydrogenation properties were followed by thermogravimetric analysis coupled to mass spectrometry.

2. Materials and methods

2.1. Materials

Hydrazine borane $N_2H_4BH_3$ (HB) was synthesized according to a protocol we previously optimized [13]. Calcium hydride CaH_2 (98%) purchased from Alfa Aesar was used as received. Both chemicals were stored and systematically handled in an argon-filled glove box (MBraun M200B, with O_2 < 0.1 ppm and H_2O < 0.1 ppm).

2.2. Preliminary comment

In the present project, we first attempted to synthesize $Ca(HB)_2$ via a wet chemistry approach. Anhydrous tetrahydrofuran (THF; ≥99.9%; Sigma-Aldrich) was used. Under argon atmosphere (i.e. in the glove box) and at room temperature, 50 mg of HB (1.09 mmol) was dissolved in 10 mL of THF. In parallel, 23 mg of CaH_2 (0.546 mmol) was dispersed in 10 mL of THF. The borane solution was slowly added to the hydride dispersion. The mixture was allowed to age for 48 h under stirring. After solvent extraction, a solid consisting of unreacted HB and CaH_2 was recovered. This synthesis approach was thus abandoned, and we returned to our solid-solid reaction approach.

2.3. Temperature-dependent evolution of CaH_2-2HB

The synthetic conditions for $Ca(HB)_2$ were defined as follows. Under argon atmosphere, 275 mg of CaH_2 (6.5 mmol) and 600 mg of HB (13 mmol) were put in a stainless steel jar of 50 mL (containing 12 g of stainless steel balls) and mixed at 200 rpm for 10 min (Retsch PM 100 planetary mill). The resulting mixture, denoted **1**, was recovered to be stored under argon atmosphere. In another argon-filled glove box (MBraun Unilab, O_2 < 0.1 ppm and H_2O < 0.1 ppm), **1** was loaded into a glass capillary of 0.5 mm diameter. The capillary was sealed to prevent the sample from air and moisture. **1** was analyzed by X-ray thermodiffractometry using synchrotron radiation (Swiss Norwegian Beam Line SNBL BM01A, at European Synchrotron

Facility ESRF, Grenoble, France). The diffraction patterns were collected using a monochromatic beam and a PILATUS 2M detector. NIST standard LaB_6 was used for the calibration of all the parameters of the detector, the sample-detector distance (343.71 mm), and the wavelength of 0.70814 Å. The temperature change was controlled with an Oxford Cryostream 700+ allowing working over the range of temperature 19-100°C. The diffraction patterns were recorded simultaneously using a rotation of the capillary of 60° min^{-1}. In parallel, **1** was analyzed by differential scanning calorimetry (DSC; Q600, TA Instruments). The sample was heated from 0 to 75°C at 1°C min^{-1}, and then it was cooled down to 0°C at the same rate.

On the basis of the aforementioned thermodiffraction and DSC experiments, **2** (in fact a $Ca(HB)_2$-rich sample) was synthesized from **1**. Typically, **1** was loaded in a stainless reactor under argon atmosphere (in the glove box) and then sealed. The sample was heated up to 62°C at 1°C min^{-1}, kept at this temperature for 50 min, and quickly cooled down (by immersing the reactor in a tap water bath). The as-formed **2** was recovered and stored in the argon-filled glove box.

2.4. Characterization of $Ca(HB)_2$

Two XRD patterns among those collected were selected to be solved and indexed. The first pattern was that obtained at 19°C for **1** and consists in a mixture of CaH_2 and HB. It was refined using the Rietveld method to confirm the proportion of the two phases (cf. SI). The second pattern was the one collected at 62°C; it belongs to **2** that was found to consist in a mixture of $Ca(HB)_2$ and CaH_2. The unit cell parameters of $Ca(HB)_2$ were determined using DICVOL06 [24]. Starting from the determined parameters, the structural model of $Ca(HB)_2$ was obtained by using FOX [25]. The as-obtained model was refined using the JANA2006 software package [26]. The Rietveld refinement was carried out considering the two phases, $Ca(HB)_2$ and CaH_2, while for $Ca(HB)_2$ the fragments N−N−B were considered as being two different molecular fragments and as being rigid. The Rietveld refinement was carried out using a Pseudo-Voigt peak shape with a cut-off of 12 for the two phases. Considering the quality of the diffraction pattern, the isotropic thermal parameters (B_{iso}) were constrained to be identical for the same atom type in the unit cell. The locations of the H atoms linked to the N and B atoms were determined by performing a geometry constrained optimization of the structure (Ca, B and N atoms fixed in their initial positions) at the force-field level. All atoms of the system were represented as Lennard-Jones

charged sites with LJ parameters taken from the UFF force field [27] while the charges were calculated using the QeQ [28] method. In addition, the uncertainties of the atomic coordinates for the H atoms are not reported here because they were not refined.

2 was analyzed by magic-angle spinning nuclear magnetic resonance (MAS NMR) spectroscopy on the nuclei ^{11}B (Varian VNMR400; 128.37 MHz; 20000 rpm) and [43]Ca (Varian VNMR600; 40.37 MHz; 20000 rpm). To this end, **2** was loaded in the NMR rotor in the glove box. The rotor was afterwards put in an argon-filled vial (to prevent the sample from air and moisture) and transferred to the spectrometer localized in another building. The NMR analyses were performed at $-10°C$. **2** was also analyzed by Fourier transform infrared spectroscopy (FTIR; IS50 Thermo Fisher Scientific). The thermal behavior of **2** was studied by thermogravimetric (TG) analysis (Netzsch STA 449 F1 Jupiter) coupled to mass spectrometry (MS; Netzsch QMS 403D Aëolos Quadro) and by differential scanning calorimetry (DSC; Q600, TA Instruments). The heating rate was $1°C$ min^{-1} and the analyses were performed up to 300°C.
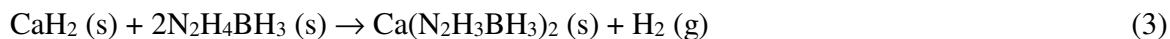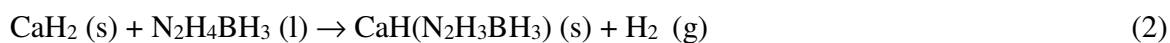
The thermolytic residue, denoted **3**, forming upon the decomposition of **2** at 200°C was prepared in high amount for analysis. Typically, **2** was loaded in a stainless reactor under argon atmosphere and sealed. It was heated up to 200°C at $1°C$ min^{-1}. Then it was allowed to cool down. The as-obtained **3** (recovered in the argon-filled glove box) was analyzed by powder X-ray diffraction (XRD; PANalytical X'Pert Multipurpose diffractometer equipped with an X'Celerator detector; Cu $K\alpha_1/\alpha_2$ radiation, $\lambda = 1.5418$ Å, 45 kV, 30 mA). The XRD pattern was collected using Bragg-Brentano geometry on a spinning zero background sample holder loaded in the glove box. The powder was protected using a Kapton foil stuck onto the sample holder with Apiezon grease (H quality) to prevent any air and moisture contamination. **3** was also analyzed by ^{11}B MAS NMR and FTIR spectroscopy.

3. Results and discussion

3.1. Synthesis of Ca(HB)$_2$

Though the coveted Ca(HB)$_2$ was elusive in our previous attempts [21], the TG analysis results of the binary mixture CaH$_2$-2HB opened up a new possibility. An interesting feature was the

evolution of some H_2 starting from about 60°C, which was interpreted as a possible reaction of CaH_2 with melted HB, in some extent, such as:

$$CaH_2 \text{ (s)} + N_2H_4BH_3 \text{ (l)} \rightarrow CaH(N_2H_3BH_3) \text{ (s)} + H_2 \text{ (g)} \qquad (2)$$

$$CaH_2 \text{ (s)} + 2N_2H_4BH_3 \text{ (s)} \rightarrow Ca(N_2H_3BH_3)_2 \text{ (s)} + H_2 \text{ (g)} \qquad (3)$$

The key to synthesize $Ca(HB)_2$ appeared to be the temperature. Then, our further efforts, through the present work, focused on the use of in situ synchrotron X-ray thermodiffraction to validate our assumption and to find the temperature at which the sought phase $Ca(HB)_2$ could be obtained.

We prepared a mixture of one equivalent of CaH_2 and two equivalents of HB, ball-milled at 200 rpm for 10 min under argon atmosphere. The as-obtained homogeneous mixture, denoted **1**, was heated at 1°C min^{-1}, starting from 19°C. The temperature evolution of **1** was analyzed by thermodiffraction up to 100°C (Figure 1 and S1). The thermodiffraction data were analyzed in conjunction with the DSC results (collected over the temperature range 0-75°C) (Figure 2). Below 45°C, the diffraction peaks can be all assigned to the CaH_2 and HB phases. For example, the XRD pattern collected at 19°C was refined using the Rietveld method (Figures 3 and S2, Table S1). The unit cell parameters and atomic positions for the two phases, i.e. HB and CaH_2, were found to be in good agreement with those published previously [13,29]. The relative amounts of the HB and CaH_2 solids obtained by the refinement of the powder XRD data were 27.9(5) and 72.1(2) wt%, leading to a molar ratio of 2.36.

Beyond 45°C, a baseline deviation of the heat flow is observed, suggesting an exothermic reaction. Concomitantly, new diffraction peaks appear, for example between 4 and 10°, and they grow with the increase of the temperature. Their apparition is correlated with the decrease of the intensity of the peaks of both CaH_2 and HB. In other words, a new phase, denoted **2**, is forming.
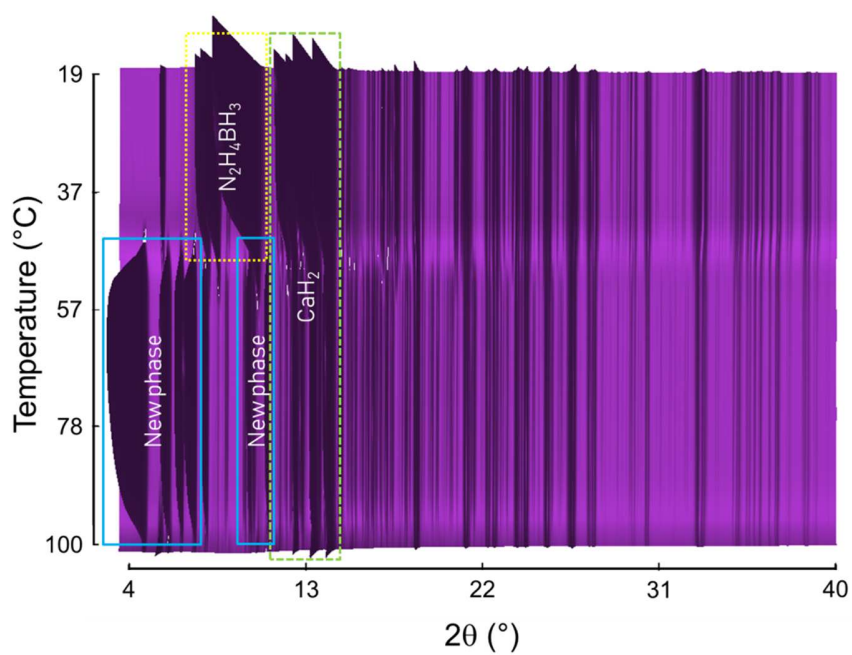
Figure 1. Sequential plot of the diffraction patterns obtained from **1** (the mixture of 1 equiv CaH_2 and 2 equiv HB) within the temperature range 19-100°C. The new phase is $Ca(HB)_2$.
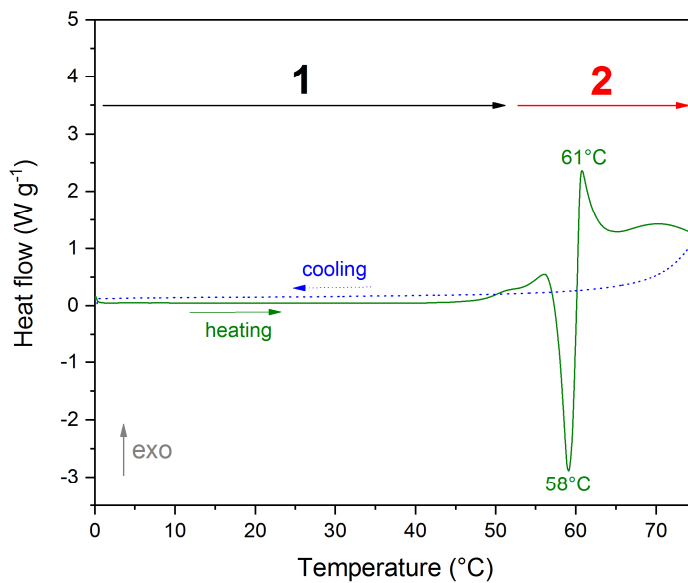

Figure 2. DSC analysis of **1** upon heating up to 75°C and then cooling down to 0°C (heating rate of 1°C min^{-1}). The temperature ranges of the samples **1** and **2** are shown.
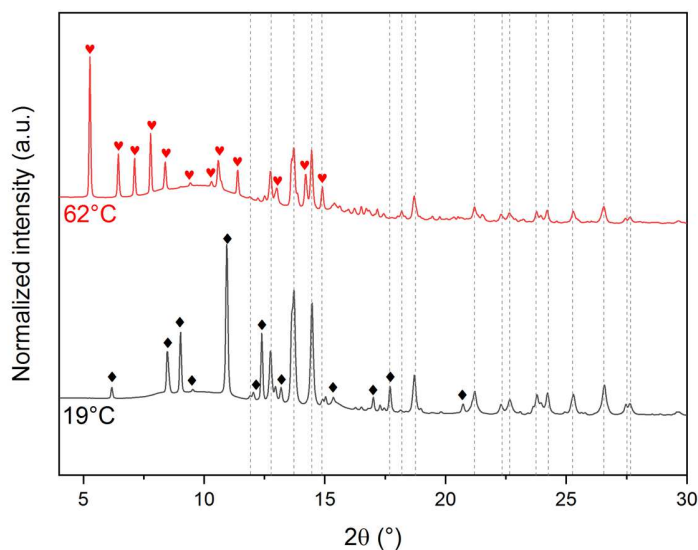
8

Figure 3. X-ray diffraction patterns of **1** collected at 19°C and 62°C. The main peaks belonging to CaH_2 (vertical dashed grey lines) and HB (symbol ♦) are shown (indexed pattern shown by Figure S2). The main peaks due to the new phase $Ca(HB)_2$ are indicated by the symbol ♥ (indexed pattern shown by Figure S3).

Above 55°C, the aforementioned exothermic event is compensated by an endothermic event that is typical of HB melting, but the exothermic signal gets rapidly over the endothermic one. Under cooling from 75°C down to 0°C, neither exothermic signal nor endothermic one is seen, bearing out the formation of the new phase. The key to synthesize $Ca(HB)_2$ seems to be the temperature, more precisely it seems to be HB in liquid state (leading to increased entropy factor) that is more likely to react with solid-state CaH_2. Peaks due to a small amount of unreacted CaH_2 can be seen above 55°C, which indicates that **2** would be a mixture of the new solid as the main phase (i.e. $Ca(HB)_2$) and of some CaH_2. Similar phase-rich solids were reported for the amidoborane counterpart $Ca(NH_2BH_3)_2$ that was prepared by ball-milling [30,31]. An additional experiment using Beyond 97°C, the diffraction peaks of **2** cannot be observed anymore, suggesting decomposition.

3.2.   Crystal structure of Ca(HB)₂

The XRD pattern corresponding to the maximum intensity of **2** (i.e. that collected at 62°C) was successfully indexed using a mixture of two phases (Figures 3 and S3). The first phase is CaH_2, indexed as an orthorhombic *Pnma* (No. 62) unit cell [29]. The second one is $Ca(HB)_2$, indexed as a monoclinic *Ic* (No. 9) unit cell. The relative amounts of these two crystalline phases are 29.0(7)

9

and 71.0(3) wt%, respectively, as obtained by the refinement of the XRD pattern. The structure parameters corresponding to Ca(HB)$_2$ (as well as those of the remaining CaH$_2$) are summarized in Table 1.

The HB derivatives show the same lattice system, i.e. monoclinic, but Ca(HB)$_2$ shows a different cell (s.g. Ic versus $P2_1/n$ for NaHB [20]). As a derivative of AB, Ca(NH$_2$BH$_3$)$_2$ shows a different monoclinic cell (s.g. $C2$ (No. 5)) [30]. Besides it shows a smaller cell volume per formula unit (138.5 Å^3) compared to that of Ca(HB)$_2$ (244.8 Å^3); this is consistent with the larger size of the anion [N$_2$H$_3$BH$_3$]$^-$. The volume per formula unit of HB is also smaller with 80.2 Å^3 [13]; this is consistent with the presence of the bulkier cation Ca^{2+} in Ca(HB)$_2$.

According to the derived crystal structure of Ca(HB)$_2$ (Figures 4 and 5), the intermolecular interactions form chains (layers) along the a axis. The Ca···Ca distance along the a axis (intra-chain) is the shortest one, with 4.39 Å, whereas the inter-chain Ca···Ca distance is 7.04 Å. The shortest Ca···N distance is 2.53 Å, which is comparable to that in Ca(NH$_2$)$_2$ (2.44-2.57 Å) [32] and is slightly longer than the shortest distance in Ca(NH$_2$BH$_3$)$_2$ (2.47 Å) [30]. The shortest Ca···B distance is 3.38 Å, whereas distances of 2.87-3.03 and 2.89-2.96 Å were reported for Ca(NH$_2$BH$_3$)$_2$ [30] and Ca(BH$_4$)$_2$ [33] respectively. The Ca···H–B and Ca···H–N distances resulting from the geometry optimization are between 2.33 and 2.43 Å. With respect to the two directly binding anions, the distances of the N–N bonds from the Rietveld refinement are 1.38 and 1.40 Å. They are comparable to the distance observed for HB (1.41 Å) [13], but shorter compared to the MHBs (α-LiHB 1.47 Å [17]; β-LiHB 1.50 Å [18]; NaHB 1.46 Å [19]; KHB 1.47 Å [22]; RbHB 1.43 Å [23]). The B–N bonds have lengths of 1.53 and 1.57 Å. This is consistent with the bond lengths in Ca(NH$_2$BH$_3$)$_2$ (1.55 Å) [30] and in the MHBs (1.54-1.55 Å) [17,18,19,22,23]. They are all slightly shorter than the B–N bond of HB (1.59 Å) [13]; this is typical of the bond strengthening/shortening due to M$^+$ or M^{2+} insertion. With regard to the interactions between the [N$_2$H$_3$BH$_3$]$^-$ anions, the average intermolecular H$^{\delta+}$···H$^{\delta-}$ distance is about 2.16 Å, which is longer than the distance in HB (2.01 Å) and shorter than the sum of the van der Waals radii for two H atoms (2.4 Å) [13]. These interactions, together with the van der Waals interactions between the cation and the anionic entities, take part to the stabilization of the solid state of Ca(HB)$_2$ [34].

Table 1. Space groups (*s.g.*), unit cell parameters, goodness of fit (GoF), R values, and structural parameters for the refined structures Ca(HB)$_2$ and CaH$_2$ in **2**.

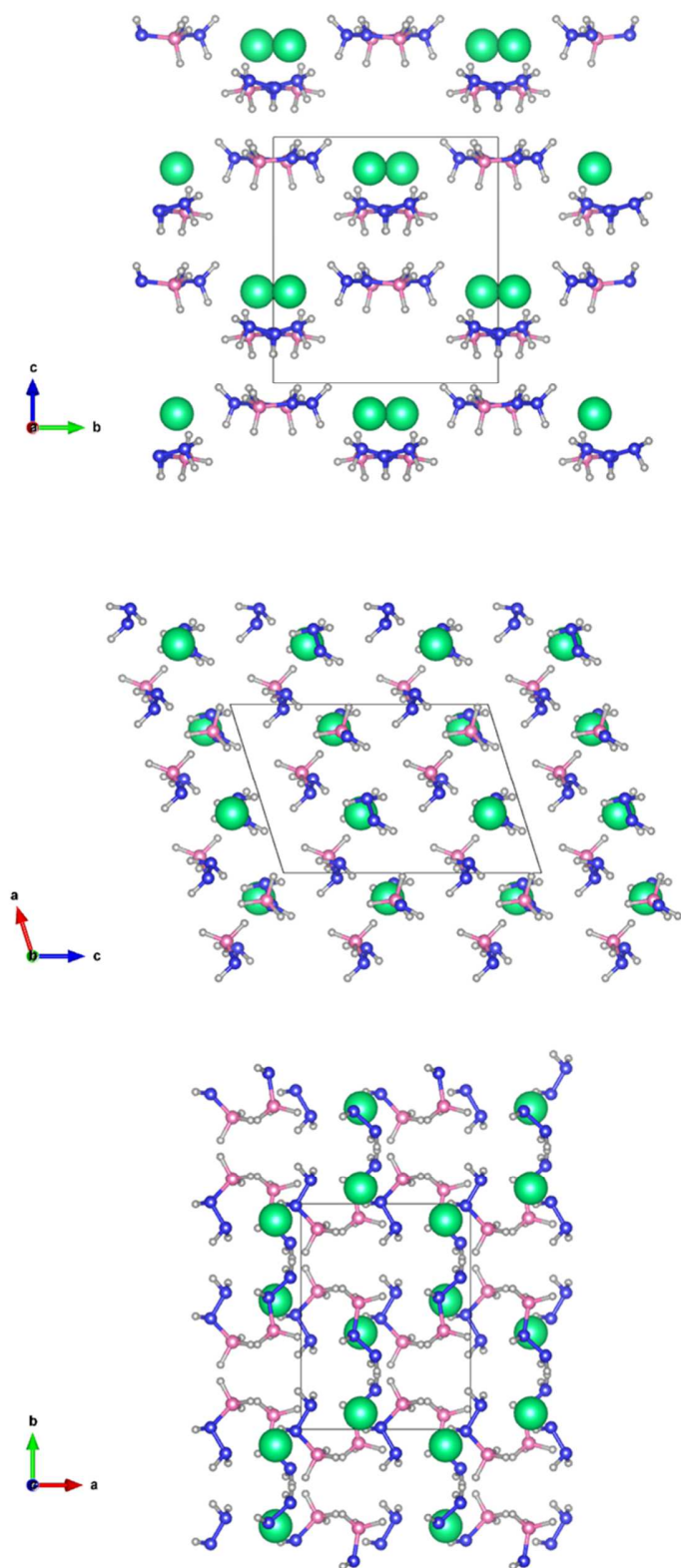| Formula	Ca(NH$_2$NHBH$_3$)$_2$					
s.g.	*Ic* (No. 9)					
Z	4					
a (Å)	8.2597(12)					
b (Å)	10.4118(15)					
c (Å)	11.9367(17)					
β (°)	107.515(10)					
V (Å^3)	979.0(3)					
Temperature	62°C					
R$_{(obs)}$ / wR$_{(obs)}$	16.39 / 20.88					
R$_{(all)}$/wR$_{(all)}$	16.42 / 20.89					
Atom	**Site**	**Occupancy**	**x**	**y**	**z**	**Biso (Å^2)**
Ca1_1			0.3524(11)	0.4290(14)	0.8726(6)	0.072(5)
B1_1			0.599(6)	1.112(4)	0.195(4)	0.015(12)
N2_1			0.559(4)	0.894(3)	0.230(3)	0.036(8)
N3_1			0.471(4)	1.008(3)	0.201(3)	0.036(8)
H1_1			0.70568	0.12429	0.28649	1.2
H2_1			0.52889	0.21314	0.17802	1.2
H3_1			0.65159	0.09379	0.11456	1.2
H4_1			0.48451	0.66868	0.76230	1.2
H5_1			0.57346	0.64977	0.65428	1.2
H6_1	4e	1	0.38265	0.50134	0.61936	1.2
B2_1			0.341(8)	-0.062(4)	0.901(4)	0.015(12)
N4_1			0.439(4)	0.173(3)	0.915(3)	0.036(8)
N5_1			0.311(4)	0.085(3)	0.915(3)	0.036(8)
H7_1			0.32078	0.58609	0.30016	1.2
H8_1			0.48034	0.58979	0.45625	1.2
H9_1			0.24546	0.62381	0.43558	1.2
H10_1			0.91255	0.70923	0.32978	1.2
H11_1			0.94848	0.74196	0.47977	1.2
H12_1			0.74850	0.60788	0.47658	1.2
Formula	**CaH$_2$**					
s.g.	*Pnma* (No. 62)					
Z	4					
a (Å)	5.9663(5)					
b (Å)	3.6053(3)					
c (Å)	6.8233(6)					
V (Å^3)	146.77(2)					
Temperature	62°C					
R$_{(obs)}$ / wR$_{(obs)}$	8.44 / 16.95					
R$_{(all)}$/wR$_{(all)}$	8.44 / 16.95					
Atom	**Site**	**Occupancy**	**x**	**y**	**z**	**Biso (Å^2)**
Ca1_2	4e	1	0.2626(11)	0.75	0.1104(4)	0.0104(9)
GoF	25.79					
Rp	2.25					
wRp	2.78					

Figure 4. Crystal structure of Ca(HB)$_2$ along the *a*, *b* and *c* crystallographic axes. The white, pink, blue and green spheres correspond to the H, B, N and Ca atoms respectively.

As mentioned in the introduction, Wu et al. [17] attempted a synthesis of $Ca(HB)_2$ by ball-milling CaH_2 and HB (mol ratio 1:2) at 200 rpm for 3h. They reported a partial XRD pattern without further exploitation. We compared it to the pattern we collected here: some of the peaks are comparable to ours for a 2θ range likely between 5 and 15°, and the others look like belonging to unreacted HB. In other words, Wu et al. were able to recover a $Ca(HB)_2$-containing solid by using a planetary mill (Fritsch Pulverisette 7), whereas we failed to synthesize it by using a different planetary mill (Retsch PM 100) [21]. Interestingly, with respect to the polymorphic LiHB, Wu et al. [17] synthesized the high-temperature phase with their planetary mill, whereas we synthesized the low-temperature phase with ours. These two different achievements indicate first that the device used by Wu et al. is more energetic in comparable milling conditions, and second that synthesis of a HB derivative is also sensitive to the apparatus used.
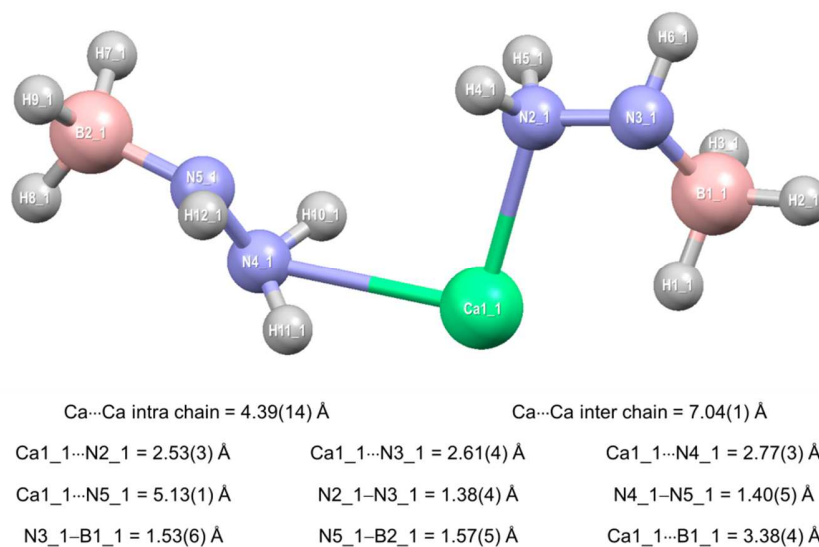

Ca···Ca intra chain = 4.39(14) Å   Ca···Ca inter chain = 7.04(1) Å

Ca1_1···N2_1 = 2.53(3) Å   Ca1_1···N3_1 = 2.61(4) Å   Ca1_1···N4_1 = 2.77(3) Å

Ca1_1···N5_1 = 5.13(1) Å   N2_1–N3_1 = 1.38(4) Å   N4_1–N5_1 = 1.40(5) Å

N3_1–B1_1 = 1.53(6) Å   N5_1–B2_1 = 1.57(5) Å   Ca1_1···B1_1 = 3.38(4) Å

Figure 5. Asymmetric unit showing the coordination around the cation Ca^{2+}, and inter- and intra-atomic distances obtained for $Ca(HB)_2$ in **2**.

3.3. Molecular analysis of $Ca(HB)_2$

2 was analyzed by ^{11}B MAS NMR spectroscopy (Figure 6). The spectrum shows a single split signal centered at −24 ppm, typical of a quadrupolar coupling for an N*B*H$_3$ environment. The electron repartition around the B element is anisotropic. This is different from the isotropy and the single Gaussian-like signal reported for the alkali derivatives, where the strong interaction

between M^+ (M = Li, Na, K) and BH_3 substantially smooths the electronic repartition around B [17,18,20,22]. With **2**, the larger atomic size and lower electropositivity of Ca^{2+} would make the $Ca^{2+} \cdots H^{\delta-}-B$ interactions weak enough not to modify the anisotropic repartition of electrons around B [9,10]. Our observation is in fact consistent with the signature reported for $Ca(NH_2BH_3)_2$ [35]. The spectrum of **2** shows a small deviation of the baseline between 0 and -15 ppm ascribed to N_2BH_2 and N_3BH environments that we usually see because of the high-speed rotation of the spectrometer rotor. However, we cannot discard dehydrocoupling in small extent of HB molecules when **1** was heated.
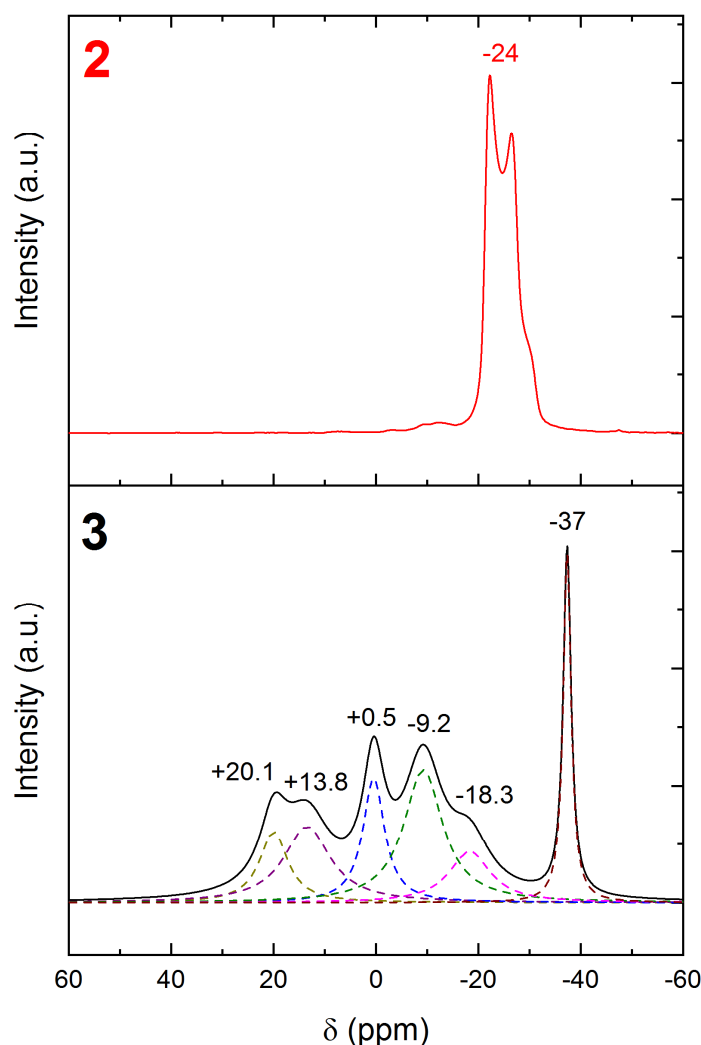

Figure 6. ^{11}B MAS NMR spectra of **2** and **3**. The chemical shifts (in ppm) of the signals are given. For **3**, the deconvoluted signals are shown in dashed lines.

14

2 was also analyzed by ^{43}Ca MAS NMR spectroscopy (Figure 7). The spectrum shows one broad and asymmetric signal which maximum is at 58.1 ppm. It cannot be ascribed to CaH$_2$ (+94.4 ppm) [36]. The chemical shift of the nucleus ^{43}Ca is sensitive to the (Pauling) electronegativity of the element with which Ca^{2+} interacts. As Ca^{2+} interacts with N (χ_N = 3.04) of the anion [N$_2$H$_3$BH$_3$]$^-$, the signal belonging to **2** is expected to appear at lower chemical shift (+58.1 ppm) than the signal due to CaH$_2$ (+94.4 ppm; χ_H = 2.2) and at higher chemical shift than that for e.g. CaF$_2$ (−1.4 ppm; χ_F = 3.98) [37]. These observations support the formation of **2**. The presence of an additional signal of low intensity at +71.4 ppm, i.e. between the signal ascribed to **2** and that of CaH$_2$, cannot be discarded. It may belong to an intermediate species such as HCa(N$_2$H$_3$BH$_3$) (Eq. 2).
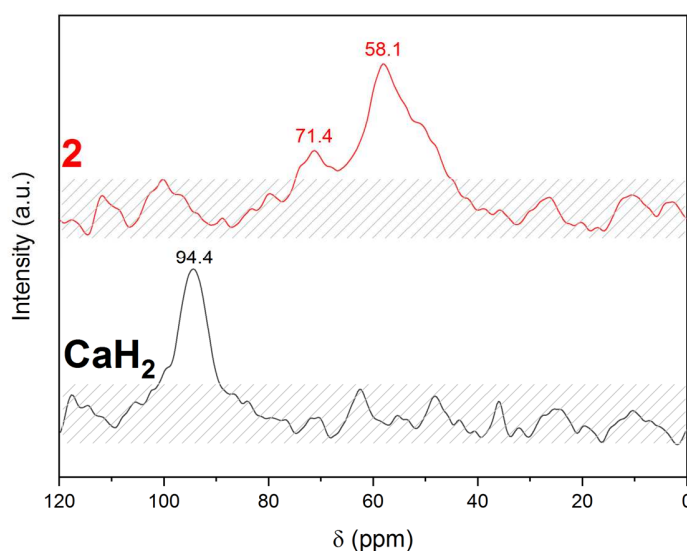

Figure 7. ^{43}Ca MAS NMR spectra of **2** and of CaH$_2$. The chemical shifts of the prominent signals are given. The hatched area aims at distinguishing the possible signal at +58.1 ppm in the background noise.

2 was analyzed by FTIR spectroscopy (Figure 8). The spectrum is typical of a compound containing N−H, B−H, N−N and B−N bonds. The vibrational modes of N−H are represented by the bands at 3500-2500 cm^{-1} for symmetric and asymmetric stretching, and 1650−1300 cm^{-1} for asymmetric and symmetric wagging. The band at 1334 cm^{-1} has been assigned to N−N bending and that at 100-940 cm^{-1} for twisting and/or rocking. The vibrational modes of B−H can be seen

through the bands at 2500-2100 cm^{-1} for symmetric and asymmetric stretching, and at 1300–1100 cm^{-1} for wagging and/or rocking. The N−N bond is mainly characterized by the band present at 1000 cm^{-1} (stretching). The B−N bond can be seen *via* the symmetric stretching mode at 746 cm^{-1}. Compared to the spectrum of HB [13], the B−H stretching bands of **2** show red shifts, indicating weakened B−H bonds. The N−H stretching region is as complex, with bands showing blue (2950 cm^{-1}), red (3210 and 3033 cm^{-1}), or negligible (3330, 3268 and 2661 cm^{-1}) shifts. This is consistent with cation-induced changes in the electronic densities of the anion [N$_2$H$_3$BH$_3$]$^-$ [15,38].
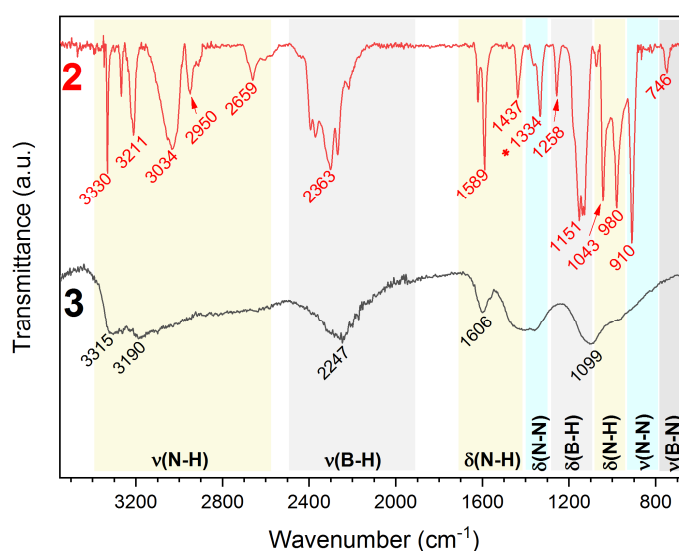

Figure 8. FTIR spectra of **2** and **3**. The vibration bands have been assigned and the wavenumbers (cm^{-1}) are shown.

3.4. Thermal analysis and dehydrogenation properties of **2**

The gravimetric hydrogen density of pure Ca(HB)$_2$ is 9.3 wt% H. The figure is high enough to consider the compound as a possible solid-state hydrogen carrier, provided it is able to release H$_2$ in mild conditions. Such a potential can be easily assessed by thermal analysis.

2 was analyzed by TG-MS and DSC over the temperature range 50-300°C at which CaH$_2$ is thermally stable (Figure 9). The curves can be divided into three distinct parts. (*i*) The part between 50 and about 90°C shows a weight gain of about 1.5 wt%. This is due to a "buoyancy" effect associated to the slow evolution of H$_2$ in an argon-filled semi-closed crucible (i.e. an

aluminum crucible sealed with a cap having a small hole); this happens when argon (heavier than H_2) is slowly expelled from the crucible while lighter H_2 forms. The H_2 release is slightly exothermic as evidenced by the very small hump on the DSC curve over the aforementioned temperature range. (*ii*) The second part of the curves starts from about 90°C and ends at about 170°C. **2** mainly dehydrogenates. The H_2 evolution followed by MS shows a maximum of intensity at 133°C. There is a concomitant release of N_2. This is in fact typical of MABs [17-22]. Volatile (unwanted) by-products like NH_3 and N_2H_4 are also generated. This indicates decomposition of **2** to some extent. The DSC curve shows a large exothermic wave, suggesting that the overall process is rather complex. (*iii*) The third part of the curves, starting from about 170 °C, is characterized by the evolution of H_2 only. At 300°C, the weight loss of **2** is 12 wt%, which is higher than the gravimetric hydrogen density of $Ca(HB)_2$ by 2.7 wt%, thus consistent with the release of N_2, NH_3 and N_2H_4 together with H_2.

It is interesting to compare the DSC curves of **2** and **1** (Figures 2 and 9). Between about 50 and 90°C, **1** shows melting (endothermic signal) and evolution (subsequent exothermic signal); **2** does not evolve (fairly stable over the temperature range). The fact remains that **1** transforms into **2**. Above 90°C, the DSC profiles of **1** and **2** are superimposable, confirming that **1** transformed into **2**.

2 does not melt. The DSC curve (Figure 9) does not show any endothermic process. We visually inspected the sample when heated up to 100°C and it did not show a change of physical state.

Dehydrogenation of B-N-H materials is generally compared at e.g. 200 °C. At such a temperature, the weight loss for **2** is 5.3 wt%. By ignoring the release of by-products, one may assume the evolution of roughly 3 equiv H_2 (out of a maximum of 6). The dehydrogenation extent of **2** is lower than that of amidoboranes [11,30,39-41] and hydrazinidoboranes [17,20,22] (Table 2). The destabilization effect of Ca^{2+} is less important than for Li^+, Na^+ and K^+. This is confirmed by the FTIR spectrum of the thermolytic residue, denoted **3**, forming upon heating **2** up to 200°C (Figure 8): the B–H and N–H vibration bands are weakened and broadened in comparison to those of **2**, but they are still relatively high in comparison to those observed for polymeric residues formed by extensive dehydrogenation of *e.g.* AB, like cross-linked

polyiminoborane and polyborazylene [42]. Interestingly, comparable thermolytic properties were reported for $Ca(NH_2BH_3)_2$, which liberated about 3.4 equiv H_2 up to 200°C [30].
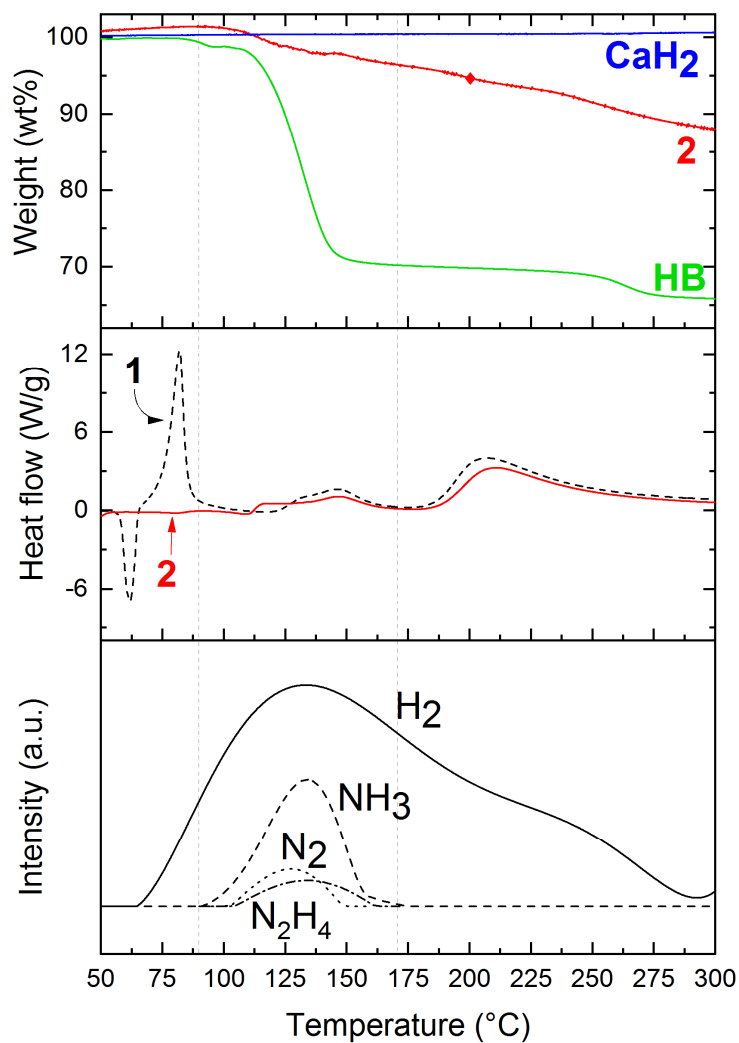

Figure 9. (top) Thermogravimetric analysis of **2**, compared to the results obtained for CaH_2 and pristine HB; the three parts mentioned in the manuscript are delimited by the vertical grey dashed lines; the symbol ♦ in red placed on the TG curve of **2** indicates the weight loss at 200°C. (middle) Differential scanning calorimetry analysis of **2**, compared to that of **1**. (bottom) Mass spectrometry analysis of the gas liberated by **2** (with H_2 m/z = 2; NH_3 m/z = 17; N_2 m/z = 28; N_2H_4 m/z = 32).

Table 2. Comparison of amidoboranes (MAB = MNH$_2$BH$_3$, and M(AB)$_2$ = M(NH$_2$BH$_3$)$_2$) and hydrazinidoboranes (MHB = MN$_2$H$_3$BH$_3$, and M(HB)$_2$ = M(N$_2$H$_3$BH$_3$)$_2$), based on their gravimetric H density (ρ_H in wt%), onset temperature of dehydrogenation (T$_{onset}$ in °C) observed by thermogravimetric analysis, dehydrogenation extent at 200°C (n$_{H2}$ per mol of anion [NH$_2$BH$_3$]$^-$ or N$_2$H$_3$BH$_3$]$^-$), and, in any, the list of the by-products found together with H$_2$.

Family	Compound	ρ_H (wt%)	T$_{onset}$ (°C)	n$_{H2}$/n$_{anion}$	By-products	Ref.
MAB	LiAB	13.7	ca. 70	1.9	none	[39]
	NaAB	9.5	ca. 57	2	none or NH$_3$ [a]	[11,40]
	KAB	7.3	ca. 66	2	none	[41]
M(AB)$_2$	Ca(AB)$_2$	10.1	ca. 75	1.7 [b]		[30]
MHB	LiHB	11.7	ca. 70	2.4	N$_2$, NH$_3$	[17]
	NaHB	8.9	ca. 60	2.6	N$_2$, NH$_3$, N$_2$H$_4$	[20]
	KHB	7.2	ca. 50	3	N$_2$, NH$_3$	[22]
M(HB)$_2$	Ca(HB)$_2$	9.3	ca. 64	1.5 [c]	N$_2$, NH$_3$, N$_2$H$_4$	Present work

[a] There is a contradiction about the purity of H$_2$ in ref. [11] vs. ref. [40].
[b] i.e. 3.4 equiv H$_2$ for 1 equiv Ca(AB)$_2$.
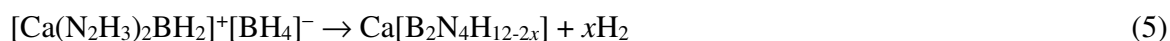[c] i.e. 3 equiv H$_2$ for 1 equiv Ca(HB)$_2$.

The thermolytic residue **3** mentioned above is mostly amorphous (Figure S4). This is typical of any dehydrogenated B-N-H materials. Few diffractions peaks of very low intensity can however be seen. They are possibly attributed to CaH$_2$. Given that CaH$_2$ in pristine state is stable up to 300°C (Figure 9), the significant decreases of the CaH$_2$ diffraction peaks from **2** to **3** suggests that, between 100 and 200°C, CaH$_2$ would have reacted with the [NH$_2$BH$_3$]$^-$ anions. The few diffraction peaks may also be interpreted as the occurrence of another minor phase like calcium borohydride Ca(BH$_4$)$_2$ [43]. **3** is of complex composition as evidenced by the presence of several boron resonances in the ^{11}B MAS NMR spectrum (Figure 6). One highly hydrogenated environment with *B*H$_4$ (−37 ppm) is attributed to in situ formed BH$_4$$^-$; it may belong to Ca(BH$_4$)$_2$, which is known to be stable up to ca. 350 °C. Its formation could rationalize the low dehydrogenation extent discussed above. The spectrum also shows N*B*H$_3$, N$_2$*B*H$_2$, and/or N$_2$*B*H environments (−18.3 and −9.2 ppm). They are typical of oligomeric/polymeric molecules with the structural units [−NH$_2$BH$_2$−] and [−NHBH−], and for which the terminal group is N*B*H$_3$ [6]. At positive chemical shift, there is a first signal at +0.5 ppm. It is ascribed to a *B*N$_4$ environment [44]. Tri-coordinated boron elements with *B*N$_3$ (+13.8 ppm) and *B*N$_2$H (+20.1 ppm) environments are also distinguished. They are typical of polyborazylene-like compounds [45]. Such a complex composition is problematic for the development of an efficient regeneration path.

Little is known about the dehydrogenation and/or decomposition paths of MHB leading to the aforementioned polymeric residues. The overall path of dehydrocoupling is complex. For example, it has been demonstrated that heteropolar H$^{\delta+}$···H$^{\delta-}$ and homopolar H$^{\delta-}$···H$^{\delta-}$/H$^{\delta+}$···H$^{\delta+}$

reactions competitively occur [46,47] resulting in NBH$_3$, N$_2$$BH_2$, N$_2$$BH, BN_3$, BN$_2$H, and BN$_4$ environments. Otherwise, we may try to clarify the likely presence of Ca(BH$_4$)$_2$ as by-product. We hypothesize the formation of [Ca(N$_2$H$_3$)$_2$BH$_2$]$^+$[BH$_4$]$^-$ as intermediate by Ca^{2+}-mediated hydride transfer from BH$_3$ of one [N$_2$H$_3$BH$_3$]$^-$ anion to BH$_3$ of the other anion, the transfer being accompanied by a scission of the N$-$B bond of the latter anion:

Ca(NH$_2$BH$_3$)$_2$ $\rightarrow$ (N$_2$H$_3$BH$_3$)Ca$-$H$\cdots$H$-$N$_2$H$_2$BH$_2$

$$\rightarrow [BH_4]^-[Ca(N_2H_3)(N_2H_3BH_2)]^+ \rightarrow [Ca(N_2H_3)_2BH_2]^+[BH_4]^- \qquad (4)$$

The formation of such transient Ca$-$H is based on the metal ion assisted hydride transfer mechanism reported for e.g. LiHB [35,48] and Ca(NH$_2$BH$_3$)$_2$ [49]. Dehydrocoupling is suggested to take place via a major path and a minor path (where the participation of the remaining CaH$_2$ is ignored). For the major path, all of the hydrogens would be likely to participate to H$_2$ evolution, such as:

$$[Ca(N_2H_3)_2BH_2]^+[BH_4]^- \rightarrow Ca[B_2N_4H_{12-2x}] + xH_2 \qquad (5)$$

With respect to the minor path, only the (N$_2$H$_3$)$_2$BH$_2$ ligands would be involved:

$$2[Ca(N_2H_3)_2BH_2]^+[BH_4]^- \rightarrow Ca[B_2N_8H_{16-2y}] + Ca(BH_4)_2 + yH_2 \qquad (6)$$

The entities N$_2$H$_3$, that are twice more concentrated than the BH$_2$ groups, could then explain the evolution of N$_2$H$_4$, NH$_3$ and N$_2$ as volatile by-products:

$$2N_2H_3 \rightarrow 2NH_3 + N_2 \qquad (7)$$

$$2N_2H_3 \rightarrow N_2H_4 + N_2 + H_2 \qquad (8)$$
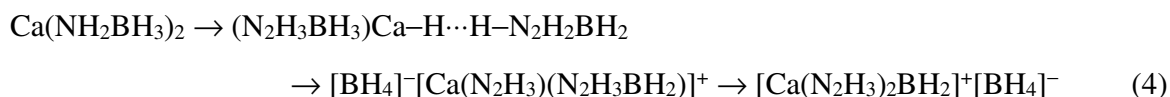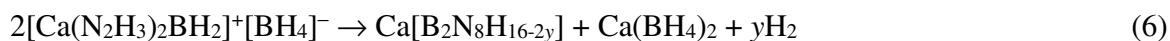
To support these mechanisms, further works, implemented by theoretical calculations, are required. Beforehand, it would be preferable to succeed in synthesizing a pure phase of Ca(HB)$_2$.

Hügle et al. [12] demonstrated that the binary mixture LiH-HB is preferable to pristine HB owing to faster dehydrogenation kinetics. It is even more attractive than LiHB on the basis of the gravimetric hydrogen density (15 and 11.7 wt% H respectively). A similar comparison can be made for **1**, our binary mixture CaH$_2$-2HB, and pure Ca(HB)$_2$. (*i*) They respectively have a gravimetric hydrogen density of 12.05 and 9.3 wt% H. (*ii*) **1** is able to release H$_2$ from about 40°C [21]: 2 equiv H$_2$ are formed by reaction of the two H$^{\delta-}$ of CaH$_2$ with one H$^{\delta+}$ of each HB molecule. Assuming that both **1** and Ca(HB)$_2$ liberate 3 equiv H$_2$ from about 100 to 200°C, the H$_2$ release capacity of **1** is then higher, with 5 equiv H$_2$ (i.e. 7.5 wt% H released). (*iii*) The weight loss at 200°C determined by TG analysis is 15.5 wt% for **1**, which supposes an important amount of N$_2$H$_4$ probably due to

some unreacted HB. Superior H_2 purity could be expected provided that improvements in the sample preparation (further optimization of the milling, mixing using a anhydrous solvent, etc.) are made. What is clear from this short comparative analysis is that any further work should focus on a pure phase of $Ca(HB)_2$ as well as on the binary mixture CaH_2-2HB.

4.   Conclusion

In situ synchrotron thermodiffraction experiments, coupled with DSC analyses, allowed us to synthesize the hitherto elusive calcium hydrazinidoborane $Ca(N_2H_3BH_3)_2$. From a binary mixture of calcium hydride CaH_2 and two equivalents of hydrazine borane $N_2H_4BH_3$, calcium hydrazinidoborane (monoclinic, s.g. *Ic*) forms above 45°C, especially at around 60°C, the temperature at which HB has melted and is liquid. The as-obtained sample is actually a mixture of $Ca(N_2H_3BH_3)_2$ as the main phase and some unreacted CaH_2. Beyond 70°C, the diffraction peaks of $Ca(N_2H_3BH_3)_2$ decay and they cannot be seen above 97°C anymore. This suggests the decomposition of the new phase, which was confirmed by thermal analyses. The calcium hydrazinidoborane-rich solid dehydrogenates within the temperature range 90-170°C, and some decomposition into volatile by-products (N_2, NH_3 and N_2H_4) also takes place. In any event, $Ca(N_2H_3BH_3)_2$ shows better dehydrogenation properties than the parent $N_2H_4BH_3$. The thermolytic residue obtained at 200°C is typical of any dehydrogenated B-N-H materials: it is amorphous and of complex composition. As it stands, $Ca(N_2H_3BH_3)_2$ may be regarded as having a potential for hydrogen storage but additional works, notably targeting a pure phase, are required. This is all the more important as further efforts might open other opportunities (e.g. boron nitride ceramics).

Acknowledgments

References

[1]   Umegaki T, Yan JM, Zhang XB, Shioyama H, Kuriyama N, Xu Q. Boron- and nitrogen-based chemical hydrogen storage materials. Int J Hydrogen Energy 2009;34:2303-11.

[2]   Li H, Tang Q, Chen X, Shore SG. Ammonia borane, past as prolog. J Organomet Chem 2014;751:60-6.

[3]   Demirci UB. Ammonia borane, a material with exceptional properties for chemical hydrogen storage. Int J Hydrogen Energy 2017;42:9978-10013.

[4]   Akbayrak S, Özkar S. Ammonia borane as hydrogen storage materials. Int J Hydrogen Energy 2018;43:18592-606.

[5]   Chiriac R, Toche F, Demirci UB, Krol O, Miele P. Ammonia borane decomposition in the presence of cobalt halides. Int J Hydrogen Energy 2011;36:12955-64.

[6]   Al-Kukhun, Hwang HT, Varma A. Mechanistic studies of ammonia borane dehydrogenation. Int J Hydrogen Energy 2013;38:169-79.

[7]   Roy B, Hajari A, Kumar V, Manna J, Sharma P. Kinetic model analysis and mechanistic correlation of ammonia borane thermolysis under dynamic heating conditions. Int J Hydrogen Energy 2018;43:10386-95.

[8]   Petit JF, Demirci UB. Discrepancy in the thermal decomposition/dehydrogenation of ammonia borane screened by thermogravimetric analysis. Int J Hydrogen Energy 2019;44:14201-6.

[9]   Chua YS, Chen P, Wu G, Xiong Z. Development of amidoboranes for hydrogen storage. Chem Commun 2011;47:5116-29.

[10]   Owarzany R, Leszczyński PJ, Fijalkowski KJ, Grochala W. Mono- and bimetalic amidoboranes. Crystals 2016;6:88.

[11]   Xiong Z, Wu G, Chua YS, Hu J, He T, Xu W, Chen P. Synthesis of sodium amidoborane ($NaNH_2BH_3$) for hydrogen production. Energy Environ Sci 2008;1:360-3.

[12]   Hügle T, Kühnel MF, Lentz D. Hydrazine borane: a promising hydrogen storage material. J Am Chem Soc 2009;131:7444-6.

[13]   Moury R, Moussa G, Demirci UB, Hannauer J, Bernard S, Petit E, van der Lee A, Miele P. Hydrazine borane: synthesis, characterization, and application prospects in chemical hydrogen storage. Phys Chem Chem Phys 2012;14:1768-77.

[14]   Moury R, Demirci UB. Hydrazine borane and hydrazinidoboranes as chemical hydrogen storage materials. Energies 2015;8:3118-41.

[15]   Aichouche A, Bouhadda Y, Bououdina M, Benyelloul K, Bentria B. The destabilising effect of alkali metal (Na and K) of hydrazine-borane $N_2H_4BH_3$ for hydrogen storage: Ab-initio study. Int J Hydrogen Energy 2018;43:14520-31.

[16]   Qian Z, Pathak B, Ahuja R. Energetic and structural analysis of $N_2H_4BH_3$ inorganic solid and its modified material for hydrogen storage. Int J Hydrogen Energy 2013;38:6718-25.

[17]   Wu H, Zhou W, Pinkerton FE, Udovic TJ, Yildirim T, Rush JJ. Metal hydrazinoborane $LiN_2H_3BH_3$ and $LiN_2H_3BH_3 \cdot 2N_2H_4BH_3$: crystal structures and high-extent dehydrogenation. Energy Environ Sci 2012;5:7531-5.

[18]   Moury R, Demirci UB, Ban V, Filinchuk Y, Ichikawa T, Zeng L, Goshome K, Miele P. Lithium hydrazinidoborane: a polymorphic material with potential for chemical hydrogen storage. Chem Mater 2014;26:3249-55.

[19]   Moury R, Robeyns K, Filinchuk Y, Miele P, Demirci UB. *In situ* thermodiffraction to monitor synthesis and thermolysis of hydrazine borane-based materials. J Alloys Compd 2016;659:210-6.

[20]   Moury R, Demirci UB, Ichikawa T, Filinchuk Y, Chiriac R, van der Lee A, Miele P. Sodium hydrazinidoborane: a chemical hydrogen-storage material. Chem Sus Chem 2013;6:667-73.

[21]   Pylypko S, Petit JF, Ould-Amara S, Hdhili N, Taihei A, Chiriac R, Ichikawa T, Cretin M, Miele P, Demirci UB. Metal hydride-hydrazine borane: towards hydrazinidoboranes or composites as hydrogen carriers. Int J Hydrogen Energy 2015;40:14975-14884.

[22]   Chua YS, Pei Q, Ju X, Zhou W, Udovic TJ, Wu G, Xiong Z, Chen P, Wu H. Alkali metal hydride modification on hydrazine borane for improved dehydrogenation. J Phys Chem C 2014;118:11244-51.

[23]   Castilla-Martinez CA, Granier D, Charmette C, Maurin G, Yot PG, Demirci UB. Rubidium hydrazinidoborane: synthesis, characterization and hydrogen release properties. Int J Hydrogen Energy, under revision.

[24]   Boultif A, Louër D. Indexing of powder diffraction patterns for low-symmetry lattices by the successive dichotomy method. J Appl Cryst 1991;24:987-93.

[25]   Favre-Nicolin V, Černý R. *FOX*, `free objects for crystallography': a modular approach to ab initio structure determination from powder diffraction. J Appl Cryst 2002;35:734-43.

[26]   Petříček V, Dušek M, Palatinus L. Crystallographic computing system JANA2006: general features. Z Kristallogr 2014;229:345-52.

[27] Rappe AK, Casewit CJ, Colwell KS, Goddard WA, Skiff WM. UFF, a full periodic table force field for molecular mechanics and molecular dynamics simulations. J Am Chem Soc 1992;114:10024-35.

[28] Rappe AK, Goddard III WA. Charge equilibration for molecular dynamics simulations. J Phys Chem 1991;95:3358-63.

[29] Takeshita HT, Oishi T, Kuriyama N. Disproportionation of $CaNi_3$ hydride: formation of new hydride, $CaNiH_3$. J Alloys Compd 2002;333:266-73.

[30] Wu H, Zhou W, Yildirim T. Alkali and alkaline-earth metal amidoboranes: structure, crystal chemistry, and hydrogen storage properties. J Am Chem Soc 2008;130:14834-9.

[31] Leardini F, Ares JR, Bodega J, Valero-Pedraza MJ, Banares M, Fernandez JF, Sanchez C. Hydrogen desorption behavior of calcium amidoborane obtained by reactive milling o calcium hydride ad ammonia borane. J Phys Chem C 2012;116:24430-5.

[32] Senker J, Muller M, Press W, Muller P, Mayer HM, Ibberson RM. Reorientational dynamics of amide ions in isotypic phases of strontium and calcium amide. 1. Neutron diffraction experiments. J Phys Chem B 1998;102:931-40.

[33] Miwa K, Aoki M, Noritake T, Ohba N, Nakamori Y, Towata SI, Züttel A, Orimo SI. Thermodynamical stability of calcium borohydride $Ca(BH_4)_2$. Phys Rev B 2006;74:155122.

[34] Luedtke AT, Autrey T. Hydrogen release studies of alkali amidoboranes. Inorg Chem 2010;49:3905-10.

[35] Li Z, He T, Wu G, Chen W, Chua YS, Guo J, Xie D, et al. Synthesis, structure and the dehydrogenation mechanism of calcium amidoborane hydrazinates. Phys Chem Chem Phys 2016;18:244-51.

[36] Dupree R, Howes AP, Kohn SC. Natural abundance solid state ^{43}Ca NMR. Chem Phys Lett 1997;276:399-404.

[37] Laurencin D, Smith ME. Development of ^{43}Ca solid state NMR spectroscopy as a probe of local structure in inorganic and molecular materials. Prog Nucl Magn Reson Spectrosc 2013;68:1-40.

[38] Li T, Zhang JG. Theoretical study of the metal-controlled dehydrogenation mechanism of $MN_2H_3BH_3$ (M = Li, Na, K): a new family of hydrogens material. J Phys Chem A 2018;122:1344-9.

[39]   Xia G, Chen J, Sun W, Tan Y, Guo Z, Liu H, Yu X. Well-dispersed lithium amidoborane nanoparticles through nanoreactor engineering for improved hydrogen release. Nanoscale 2014;6:12333-9.

[40]   Fijalkowski KJ, Grochala W. Substantial emission of NH_3 during thermal decomposition of sodium amidoborane, $NaNH_2BH_3$. J. Mater. Chem. 2009;19:2043-50.

[41]   Diyabalanage HVK, Nakagawa T, Shrestha RP, Semelsberger TA, Davis BL, Scott BL, Burrell AK, et al. Potassium(I) amidotrihydroborate: structure and hydrogen release. J. Am. Chem. Soc. 2010;132:11836-7.

[42]   Fazen PJ, Remsen EE, Beck JS, Carroll PJ, McGhie AR, Sneddon LG. Synthesis, properties, and ceramic conversion reactions of polyborazylene. A high-yield polymeric precursor to boron nitride. Chem Mater 1995;7:1942-56.

[43]   Kim JH, Jin SA, Shim JH, Cho Y W. Thermal decomposition behavior of calcium borohydride $Ca(BH_4)_2$. J Alloys Compd 2008;461:L20-2.

[44]   Kobayashi T, Gupta S, Caporini MA, Pecharsky VK, Pruski M. Mechanism of solid-state thermolysis of ammonia borane: a ^{15}N NMR study using fast magic-angle spinning and dynamic nuclear polarization. J Phys Chem C 2014;118:19548-55.

[45]   Roy B, Hajari A, Manna J, Sharma P. Supported ammonia borane decomposition through enhanced homopolar B–B coupling. Dalton Trans 2018;47:6570-9.

[46]   Wolstenholme DJ, Traboulsee KT, Hua, Y, Calhouna LA, McGrady GS. Thermal desorption of hydrogen from ammonia borane: unexpected role of homopolar B–H···H–B interactions. Chem Commun 2012;48:2597-9.

[47]   Tan Y, Chen X, Chen J, Gu G, Yu X. The decomposition of α-$LiN_2H_3BH_3$: an unexpected hydrogen release from a homopolar proton–proton pathway. J Mater Chem A 2014;2:15627-32.

[48]   Banu T, Sen K, Ash T, Das AK. Dehydrogenation of lithium hydrazinidoborane: insight from computational analysis. Int J Hydrogen Energy 2016;41:18953-162.

[49]   Kim DY, Lee HM, Seo J, Shin SK, Kim KS. Rules and trends of metal cation driven hydride-transfer mechanisms in metal amidoboranes. Phys Chem Chem Phys 2010, 12, 5446-53.

$2 \, N_2H_4BH_3$

$+$

CaH_2

$\downarrow$

$Ca(N_2H_3BH_3)_2$

$+$

H_2

5	
B	
Boron	
10.811	

7	
N	
Nitrogen	
14.007	

1	
H	
Hydrogen	
1.008	

20	
Ca	
Calcium	
40.078	

40°C

60°C

80°C

100°C